Behaviour of Electron Rings in the Early Phase After Ring Formation

W. Herrmann, J. Fink

IPP O/34 Apr.1977

MAX-PLANCK-INSTITUT FÜR PLASMAPHYSIK

8046 GARCHING BEI MÜNCHEN

MAX-PLANCK-INSTITUT FÜR PLASMAPHYSIK

GARCHING BEI MÜNCHEN

Behaviour of Electron Rings in the Early Phase After Ring Formation

W. Herrmann, J. Fink

IPP O/34 Apr. 1977

Die nachstehende Arbeit wurde im Rahmen des Vertrages zwischen dem Max-Planck-Institut für Plasmaphysik und der Europäischen Atomgemeinschaft über die Zusammenarbeit auf dem Gebiete der Plasmaphysik durchgeführt.

IPP O/34

W. Herrmann
J. Fink

Behaviour of Electron Rings in the Early Phase After Ring Formation

Abstract

The formation of electron rings and the ring behaviour just after formation are studied in a static magnetic field experiment. Particle losses and collective effects are investigated for different beam emittances, intensities and ring surroundings. The first large particle loss is connected with excessive emittance. Further losses at later times are attributed to a strong negative mass instability. This causes a spread in the energy of the electrons. At high particle numbers, if the instability is strong enough, the resulting energy and amplitude spread cannot be placed in the available space with an axial width of ± 2 cm and a radial width of ± 3 cm, and particles are lost. As the negative mass instability reaches its maximum amplitude at the investigated beam levels only 30 - 50 ns after injection, an energy ramp in the injected beam might be just as suitable for reducing the negative mass instability as an energy spread. A large instantaneous energy spread, produced by foils in the beam line, enlarges the emittance of the beam drastically.

Introduction

In electron ring experiments the formation of the rings and the phase just after it is of decisive importance for the whole experiment. Much effort has already been taken to investigate this phase /1,2,3/. But because of the complexity of the system, the dependence on many parameters, the probably mixed presence of single particle and collective effects no general recipe for the formation of good-quality rings - whatever this means - can be given. Therefore, for each new experiment this phase has to be carefully investigated.

The experiments described in the following were undertaken to prepare the Pustarex experiment /4,5/. The geometry of Pustarex is different from the other known electron ring experiments in that after injection and during compression the ring mainly moves axially. This prohibits the use of sidewalls such as have been studied in Berkeley /1/ and Garching /3/ and favours conducting cylinders as nearby walls around which the ring is formed, and along which it is moved. This geometry favours, in addition, axial inflection instead of the radial inflection always used hitherto.

The present report gives a description of the experimental apparatus in the first chapter. A discussion of the electron trapping experiments follows. As the trapping turns out to be unsufficient under many conditions the reasons for the particle losses are investigated and the losses are attributed to collective and single-particle effects. As collective effects should be reduced by enlarged energy spread, experiments were undertaken with stray foils in the beam line. A short discussion of these is given. A probable explanation for the single particle effects is found in the measurements of the beam angular divergence in the entrance snout. These are described in a separate chapter.

A few properties of the negative mass instability, especially the growth of the oscillation amplitude for different beam intensities are investigated and described. The conclusion is, that in-

stead of a large energy spread which, if produced by foils, causes large angular spreads followed by single particle losses, an energy ramp might suffice to reduce the effects of the negative mass instability and to gain (possibly a factor of 2) in the number of trapped particles.

1. Description of the Experiment

Fig.1 gives side-on and end-on sketches of the experimental arrangement. A 2 MeV electron beam is formed by a gun /6/ (1) in a Febetron Marx generator (2). The beam line (3) was shortened as much as possible to reduce the energy selectivity /7/ of the magnetic focusing lens (4) and to reduce space charge effects. A beam attenuator (5), which allows 6 different diaphragms to be used in the beam line, is followed directly by the magnetic lens. The beam line is made of normal steel with sufficient thickness to prevent the penetration of the static field.

The magnetic field is produced by two coil pairs (6,7) which are arranged to give the Pustarex field index of n = 0.45 at the injection radius of R = 20 cm (instead of R = 19 cm in Pustarex). The injection snout (8) is 3.5 cm off midplane. At R = 15 cm a copper cylinder (9) reduces the coupling impedance of the system /8/. The inflector (10) is formed by two current loops, connected in series and placed at different radii. The inner loop at R = 15 cm is cut out from the copper cylinder. The hole (axial width 8 cm, azimuthal length 12 cm) is covered by a foil with a surface resistance of 25 Ω. The outer loop is at R = 23 cm. The whole inflection system extends from $\phi = 135^{o}$ to 180^{o}. The inflector pulse used in most experiments is shown on Fig.2. There the radial field is plotted in arbitrary units versus time. The inflector field strength was set in such a way that the first particles to be trapped just barely missed the snout after the first turn. The time derivative of the inflector field was optimized by working with different maximum amplitudes of the inflector field but the same pulse length.

The conical injection snout was rolled from a 0.5 mm soft iron sheet; at the larger diameters a double sheet was taken. The opening of the snout had a diameter of 14 mm, the cone angle was 2.5°.The thickness of the iron was not enough to shield the field. Only with the currents needed for compensating the outside field disturbances, was the inner volume of the snout sufficiently field free. The current distribution for compensation in a sheet just outside the snout was found in a computer program /9/ based on the following simple argument: If the permeability of the iron is large, the field component parallel to the surface of the snout disappears. It has to be restored by the currents in the compensation sheet. If the sheet is close to the iron, the parallel field component $H_{\parallel}$ produced by the current sheet on the surface of the iron is zero and one gets from $\oint H_{\parallel} ds = I$ the relation $H_{\parallel} = j$, where the current density j on the sheet is perpendicular to $H_{\parallel}$ in the sheet. The field component perpendicular to the iron can be adjusted by current loops, wound around the snout if necessary. Fig.3 shows the current distribution calculated and used for compensation. The cylindrical and conical sheet is developed, 0° is up, 180° down and 90° is directed towards the midplane of the field. The currents on top of the cone flow from the thin to the thick end. The ends of the current paths have to be connected and this can be done via, above or below the snout and influences the perpendicular field component at the snout. If the connections are made according to the tendency of the current lines, very small additional corrections for the perpendicular field component are necessary. Field componsation to better than 1/2 % along the particle closed orbits in the midplane were obtained with this current distribution.

The vacuum vessel could be pumped to a few times 10^{-6} torr.

The particle number in the ring was obtained from the induced voltage on loops, inside (11) and outside (12) the ring (Fig.1). The size of the loops and their position were chosen such that the sum of the loop signals gave the number of electrons in the

ring almost independently of their radius or z-position. The loop is a 1 cm wide single turn coil of low inductance. (Computational checks with similar geometries suggest that the shielding of the loops reduces the signals by about 10 % which makes the particle numbers 10 % higher than given in the figures.)

2. Trapping Experiments

The main purpose of the experiment was to study the trapping of electrons in a static field with axial inflection and to get information about the main processes during the early phases of ring formation. In principle, there is no difference between radial and axial inflection. In practical, it turns out that the septum of the snout in the case of axial inflection is larger than the wall thickness because of the conical shape of the snout (with radial inflection the curvature of the ring takes care of the problem). The cone angle was therefore chosen as small as possible (2.5^{o}). If the axis of the snout is placed 3.5 cm off the midplane and if the radius of the outer tip of the snout is 1 cm, then axial amplitudes of 2.4 cm at R = 20 cm and 2.1 cm at R = 22 cm are possible. A further disadvantage might be that with multi-turn injection - as is planned - the axial width is greater than in the case of radial inflection. If the electrons are properly injected at radii corresponding to their energy, then collective and single particle radial betatron oscillations are kept small and the mentioned disadvantage of larger axial widths is counteracted by an improved radial width. In the experiment described here it was, however, not yet possible to inject all electrons at the correct particle radius.

The space available in the experiment for the rings is axially limited by the snout to about ± 2 cm, and radially by the inner copper cylinder at R = 15 cm and the outer inductive loop at R = 23 cm.

In the first experiments the number of trapped electrons after 1 μs was optimized for different inflector conditions, closed orbits and injected beam currents. The maximum injected beam current could be influenced in two ways: 1. Diaphragms with a hole on axis with different diameters d could be brought into the beam line close to the magnetic lens. This reduces the maximum current through the snout and, in addition, the angular spread of the electrons, i.e. the emittance. 2. Diaphragms with many holes, distributed over the cross-section of the beam line, could be inserted. This way the intensity is reduced but the angular spread stays constant.

Fig.4 shows the result of the trapping. Two curves are shown: curve a for reduced divergence of the beam, curve b for reduced intensity. There is a strong intensity effect (curve b), as was expected from earlier measurements with radial inflection /3,2/: the trapping efficiency decreases with increased beam current. But even at the lowest intensities the efficiency is not larger than 50 %. Higher efficiencies, however, can be obtained if the beam divergence is reduced (curve a of Fig.5). At the lowest divergences used (maximum angle d ≈ 20 mrad, see Fig.7) the number of trapped electrons reaches almost 75 % of the number of electrons injected during three turns. From Fig.4 it can therefore be concluded that the low trapping efficiency is partly caused by single particle effects because of the large divergence of the beam and partly caused by collective intensity effects. It seems worthwhile to develop beams with higher phase space density to study intensity effects in low-divergence beams.

3. Study of the Early Phases After Injection

The optimization and survey measurements described in the foregoing section already provide a hint of the origin of the early particle losses. After some improvements in the measurement with the inductive loops, a more detailed study of the early phases after injection could be undertaken. For the optimum long-time conditions of inflection the particle number in the ring just

after injection was measured as a function of time. The following technique was used: The signals of the inner and outer loops were integrated with a 600 ns decay time constant and added. A 800 MHz low pass filter in the inner loop circuit allowed to observe current oscillations up to the third harmonic of the revolution frequency (~ 250 MHz). In the outer loop circuit a 220 MHz low pass filter rejected the higher frequencies to avoid interference, if the cables were not of equal length.

Fig.5 shows the result of the ring current measurement for different intensities and divergences of the beam. The time scale is always 10 ns/div. The general behaviour is the same for all oscillograms. A rapid build-up of the current is followed by a sudden loss. Some time thereafter rf oscillations appear, which at higher intensities are connected with further losses. At the right hand side of Fig.5 three oscillograms for different intensities are shown. With the inflection method used and for betatron tunes of $\nu = 2/3$ almost three turns, i.e. about 12 ns of the injected beam can be accumulated. In the case of 100 % intensity this amounts to about 1.5×10^{13} electrons at the time of the first peak. Almost one half of the once accumulated electrons, however, is lost immediately after the third turn: it is apparently wiped off at the snout. This behaviour is the same for all intensities, even at 10 % intensity (not given in Fig.5).

This behaviour is different, however, if instead of the intensity the divergence of the beam is reduced. At the left-hand side of Fig.5 two oscillograms for reduced divergence are shown. For the lowest divergence used (a diaphragm with a diameter of d = 25 mm in the beam line) only 25 % of the once accumulated electrons are lost, that is the initial loss is only half as big as in all large divergence cases. Since for the first loss intensity effects are absent - the same 50 % initial trapping efficiency for all intensities - we conclude that it has to be attributed to single-particle effects. And even more specifically: as these losses are decreased when the beam divergence is reduced, we tend to conclude that the acceptance of the compressor is less than the beam emittance at full divergence. Measurements of the beam divergence are described in the following section.

Some time after the first loss, large amplitude oscillations appear in all oscillograms. They are attributed to the negative mass instability (see last section). As a low-pass filter of 800 MHz was used, the first three harmonics of the gyrofrequency can be seen. The amplitudes of the oscillations in the high intensity cases are much larger than in the low ones. The modulation depth for high intensities is almost 100 %.

In either case the azimuthal bunching in the ring, as manifested in the oscillations of the loop signal, should lead to a redistribution of the particle energy and consequently to beam widening. For low injected beam currents this widening is apparently so small that no further losses are incurred, whereas for large initially trapped particle numbers the large oscillations cause additional losses. If, in particular, one looks at the 100 % intensity oscillogram of Fig.5, one sees that the particle number stays at about half the maximum number for about 20 ns after the first loss, and then when the modulation of the current approaches 100 % reduces to almost one-quarter (corresponding to $\approx 4 \times 10^{12}$ electrons.

Fig.5 therefore gives some explanation of the trapping curve in Fig.4. As already assumed, the losses are partly of a single-particle nature or, more specifically, are due to excessive beam divergence and partly - at high intensities - due to collective effects manifested in current modulations that apparently cause beam widening and losses.

One more detail deserves attention in Fig.5. The oscillations do not appear immediately after injection, but need 30 - 40 ns for full development. This time corresponds to almost 10 revolutions of the electrons and is probably long enough for an energy ramp in the injected beam to suppress the negative mass instability as would an instantaneous energy spread do.

4. Measurement of Beam Divergence

As it became apparent that a large emittance of the beam prevents good trapping efficiencies, the angular divergence of the beam in the snout was measured for the different diaphragms used in the beam line. The maximum possible angle in the snout for rectilinear particle motion is given by

$$\alpha = \frac{d + d'}{2L}$$

where d is the diameter of the diaphragm, d' = 1.4 cm the diameter of the snout and L = 60 cm the distance between the snout and the focussing lens (the diaphragms were inserted close to the lens). For the different values of d used, this gives

d (cm)	α (rad)	α (^{o})
2.5	0.0325	1.86
4	0.045	2.57
6	0.062	3.53

In the experiment, the axial width of the injected beam at $\phi = 135^o$ was measured. As the field index is almost n = 0.45 and the axial betatron tune $\nu_z \simeq 2/3$, the electrons cross the midplane of the field ($B_r = 0$) at about this azimuth. For negligible energy spread, no beam divergence and constant field index over the radius the axial beam width at this azimuth would be zero. With finite axial angular spread α (in rad) in the snout one gets for the axial half-spread Δz at $\phi = 135^o$:

$$\Delta z = \frac{R \cdot \alpha}{\nu_z} = \frac{2}{3} \cdot R \cdot \alpha$$

which in this approximation does not depend on the position of the particle in the snout (R the radius of injection). With a Faraday cup, 0.5 cm wide axially and 7 cm long radially, the axial distribution of the injected current at $\phi = 135^o$ was measured (the beam was totally stopped at $\phi = 270^o$). Fig.6 gives

the result for different diaphragm apertures d in the beam line. The curves for different intensities lie, if normalized, on top of each other. One curve is shown for the insertion of a pyramid foil /6/ in the snout for an energy spread of 2 %. The foil was placed 10 cm before the end of the snout. At this position the current through the snout was reduced by the foil by a factor 2. The foil leads to a large widening of the incoming beam. If one plots the half-width half-maximum values of Δz in Fig.6 as a function of the diaphragm diameter d, one gets Fig.7. The values of α obtained from Fig.7 are not far below the maximum angles permitted by the beam line.

If the collective betatron amplitude is removed during inflection a single-particle betatron amplitude remains which is given by

$$z_1 = |(z_o - x)| \cdot \sqrt{1 + \left(\frac{\alpha R}{\nu_z (z_o - x)}\right)^2} = \Delta z_o \cdot \sqrt{1 + \left(\frac{\Delta z}{\Delta z_o}\right)^2}$$

Here x is the actual single-particle axial starting position in the snout and z_o the "collective" starting position. For large angles α and small apertures ($\frac{\Delta z}{\Delta z_o} >> 1$) one gets

$$z_1 = \Delta z.$$

If the angle α is very small $\frac{\Delta z}{\Delta z_o} << 1$, the betatron amplitude reduces to the minor snout radius $(x - z_o)$.

Owing to the large angular spread caused by the foil in the beam line the trapping efficiency of the beam with an instantaneous energy spread was very poor. It is difficult to imagine how a foil in a beam which already has a finite emittance and a time varying energy could give sufficiently good results anywhere in the beam line. Quite a few positions of the foil in the beam line have been tried, always with the same result, viz. the current through the snout was very much reduced. Only if the initial phase space density in the beam is high enough to allow for large particle losses, could a reasonably low-emittance, high-current beam be obtained.

5. Negative Mass Instability

As already discussed before, the trapping efficiency showed strong intensity effects. Two main effects were considered to be their possible origin: transverse collective and longitudinal collective instabilities. Among the transverse instabilities the most effective one should be - in the absence of resistive walls - the beam-beam instabilities as considered in /10/. These instabilities should probably be affected by image walls close to the ring. Axial and radial squirrel cages (see 13 in Fig.1) in addition to the conducting cylinder close to the ring, however, did not alter the overall trapping efficiency.

The negative mass instability therefore was the main candidate for the explanation of the intensity effects.

The negative mass instability should be absent in linear approximation if

$$N_e \leq \frac{R \cdot \gamma \cdot \left(\frac{\Delta E}{E}\right)^2}{2r_o \left| Z_m/mZ_o \right|}$$

when γ is the relativistic mass factor, $\Delta E/E$ the relative energy spread, $r_o = 2.8 \cdot 10^{-13}$ cm the classical electron radius, Z_m the coupling impedance for the m-th harmonic and $Z_o = 377\Omega$ the impedance for free space. The impedance for the low harmonics in the presence of an inner cylinder is given approximately /8/ by

$$\left| \frac{Z_m}{m} \right| = (1-s) \cdot 300$$

where s is the ratio of the cylinder radius to the ring radius. With $R \cdot \gamma = 100$ and $s \sim 0.75$ in the experiment one finds

$$N_e \leq 9 \cdot 10^{14} \left(\frac{\Delta E}{E}\right)^2 .$$

The instantaneous energy spread in the beam is very small (less than 1 %) and even the total energy spread might be as small as 1-2 %. This leads to linearly stable particle numbers of $1 - 4 \times 10^{11}$ or currents on the closed orbit as low as 4 A.

Experimentally, HF oscillations whose frequencies were equal to the gyrofrequency of the electrons and their higher harmonics were indeeed seen even for the lowest currents of about 6 A that were injected.

There are, however, differences in the oscillations between low and high-current rings: The time which elapses until the oscillations reach a certain level is longer (the growth rate is smaller) for low current beams, and the harmonic content, although not reproducible from shot to shot, is different on the average for different current levels.

Fig.8 shows the amplitude behaviour for harmonics with the number $4 \leq m \leq 8$ (corresponding to 1-2 GHz) as a function of time for different beam levels. Time zero marks the beginning of the injection. Fig.8a is for different beam intensities, 8b for different angular spreads. The maximum amplitude shifts to later times when the current level is reduced. At full beam the maximum is reached at 30 to 40 ns after injection, at 10 % beam about 70 ns after injection. The amplitude behaviour for low divergence beams in Fig.8b looks different from the other cases. An explanation cannot be given at the moment.

Fig.9 shows a typical example of the amplitude of the first harmonic as a function of time for different intensities. The "growth time" is again longer for low-level beams, but the maximum amplitudes are comparable if the 2 % case is ignored. Nonlinearities apparently limit the amplitude for the first harmonic. The amplitude of the 3rd harmonic at full beam is normally already 3 to 4 times as large as at 25% beam.

Conclusions

Experiments with beam injection into a static field with axial inflection were performed. Rings could be formed. The number of electrons in the ring was limited to about 4×10^{12}. This is about the same number of particles that could be trapped in a static field with radial inflection when the ring was formed between sideplates /3/. The experiments showed that the particle losses can be attributed to single-particle effects and to collective effects. Single-particle effects allowed formation of rings with $N_e = 8 \times 10^{12}$. To reduce the single-particle effects, a beam with lower emittance should be used (there is a small chance that an improvement in the inflection system gives better results, too). However, the overall trapping might not be increased even if the single-particle effects are avoided. The negative mass instability (with $N_e = 8 \times 10^{12}$) leads to such strong modulation and widening of the ring that half of the initially trapped electrons are lost. This loss seems to increase drastically with the particle number, with the consequence that the number of particles finally trapped might be less if the initially trapped number is increased.

The maximum number of trapped particles should increase with higher energy spread. For the present electron gun, energy spreads can be produced only by foils in the beam transport system. This, however, leads to very large beam angular spreads and to very small initially trapped particle numbers. Because, however, the time taken for the oscillations to reach an amplitude so large that additional losses are caused is a length of 5 to 6 turns, a small instantaneous energy spread together with an energy ramp might suffice - even at particle numbers of 8×10^{12} - to suppress strong effects of the negative mass instability. A ramp was used in the Berkeley experiment /1/, but a thorough investigation of this problem is not known.

The limitation of the particle number in the present experiment to something less than 4×10^{12} as compared with trapped particle numbers of 8×10^{12} in compressor I /11/ can be explained

by the fact that the space available for the ring in compressor I was axially and radially wider than the space available in this experiment. In addition, compression of the ring helps to save particles from being lost at the snout.

If the impedance of the ring surroundings cannot be reduced, energy spread and/or an energy ramp has to be applied if higher particle numbers in a ring of good quality are to be trapped.

In conclusion it can be stated that the method of ring formation with axial inflection along conducting cylinders, as it is planned for the experiment Pustarex, is applicable and leads to results which are comparable with those obtained with ring formation between sidewalls and radial inflection.

Acknowledgement

We thank Dr. C. Andelfinger for encouragement and his continuous interest in this work.

References

1 G.R. Lambertson et al., Part.Accelerators 5, 113 (1973)

2 G.V. Dolbilov et al., II.Symp.on Coll.Methods of Acceleration, Dubna 1976

V.P. Sarantsev, et al., Report of the JINR, Dubna, P9-10053 (1976)

J. Habanez, et al., Report of the JINR, Dubna, P9-9729 (1976)

3 J. Fink, W. Herrmann, W. Ott, J. Peterson, Proc.9th Int.Conf. on High Energy Accelerators, Stanford/Cal.(USA) (1974)

4 W. Herrmann, MPI f.Plasmaphysik, Garching, Report IPP O/15 (1973)

5 C. Andelfinger, et al., MPI f.Plasmaphysik, Garching, Report IPP O/30 (1976)

6 J. Fink, W. Ott, MPI f.Plasmaphysik, Garching, Report IPP O/17 (1973)

7 W. Dommaschk, private communication

8 A. Faltens, A.J. Laslett, Part.Accelerators 4, 151 (1973)

9 W. Herrmann, E. Springmann, unpublished

10 I. Hofmann, A.U. Luccio, C.E. Nielsen, MPI f.Plasmaphysik, Garching, Report IPP O/26 (1974)

11 C. Andelfinger, Part.Accelerators 5, 105 (1973)

Figure Captions

Fig.1 Side-on and end-on sketches of the experimental arrangement. Description in the text.

Fig.2 Radial component of the magnetic inflection field in arbitrary units as a function of time. Beam injection during the increasing slope after the negative peak.

Fig.3 Development of the current layer on the conical snout. 180° is radially inward, 90° towards the midplane

Fig.4 Number of finally trapped electrons $N_{e\ ring}$ as a function of injected current J_{inj}. Curve a: reduction of beam emittance. Curve b: reduction of beam intensity with constant emittance.

Fig.5 Rotating ring current in arbitrary units as a function of time in 10 ns/div. Right hand side: Variation of intensity with constant emittance. Left hand side: Reduction of emittance.

Fig.6 Axial distribution of the injected current at $\phi = 135^{\circ}$ for different diaphragm diameters d in the beam line.

Fig.7 Measured angular spreads α in the snout and corresponding minimal axial betatron amplitudes Δ_z for different diaphragm diameters d in the beam line.

Fig.8 Amplitude behaviour of the harmonics 4 to 8 of the revolution frequency (1-2 GHz) as a function of time after injection. a) for different beam intensities; b) for different beam emittances.

Fig.9 Amplitude behaviour of the first harmonic of the revolution frequency as a function of time after injection. a) for different beam intensities; b) for different beam emittances.

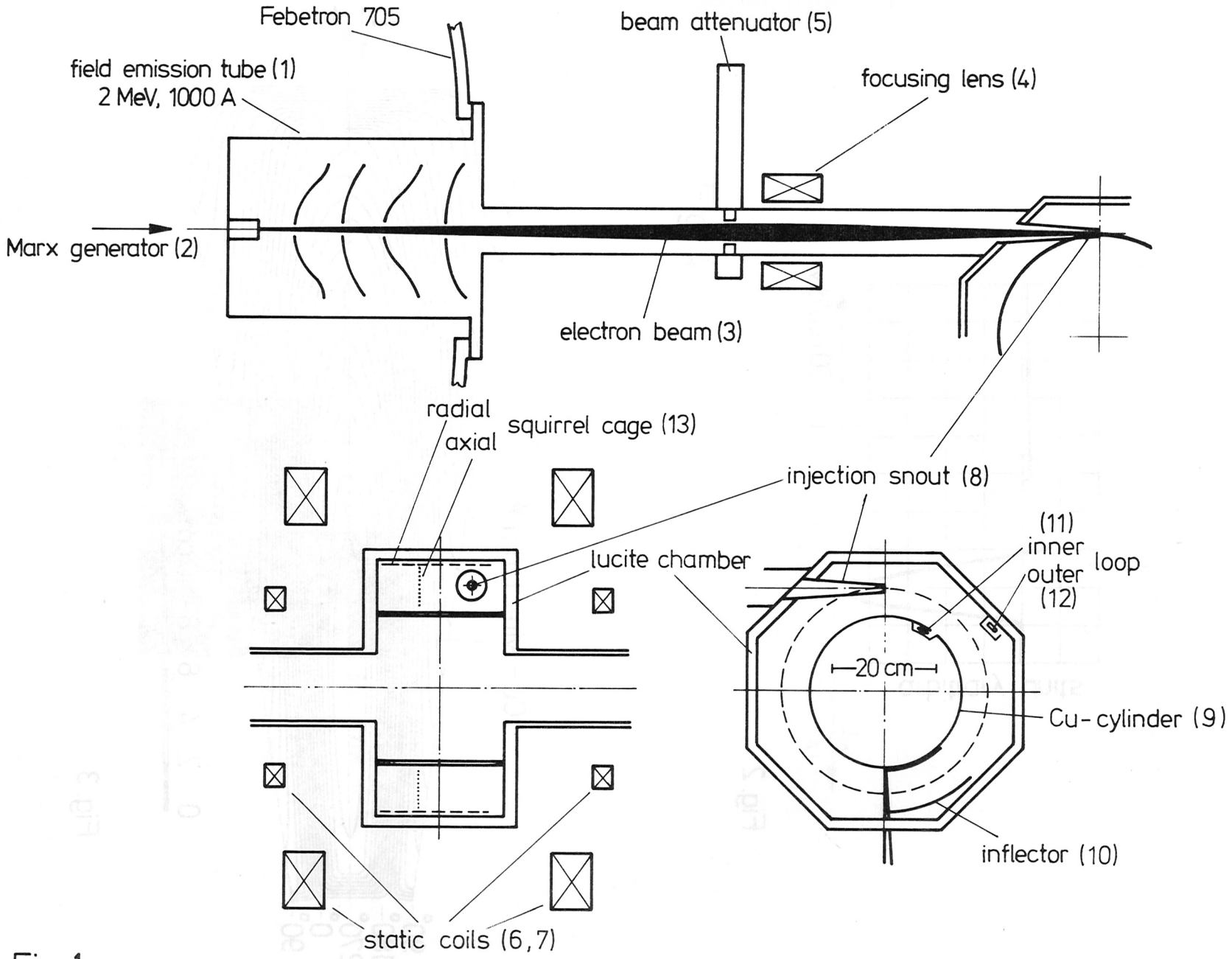
Febetron 705
field emission tube (1)
2 MeV, 1000 A
beam attenuator (5)
focusing lens (4)
Marx generator (2)
electron beam (3)
radial
axial
squirrel cage (13)
injection snout (8)
(11)
inner
outer
loop
(12)
lucite chamber
20 cm
Cu-cylinder (9)
inflector (10)
static coils (6,7)

Fig. 1

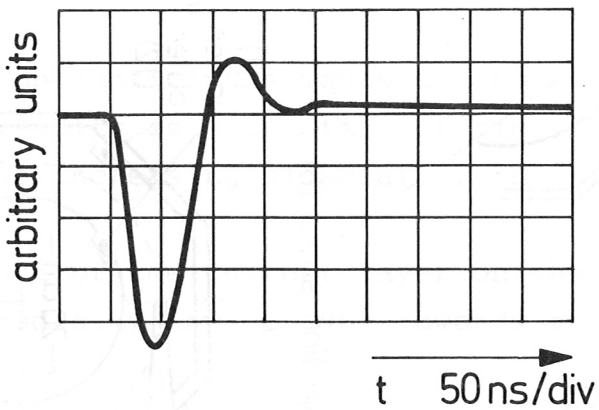
arbitrary units
t 50 ns/div

Fig. 2

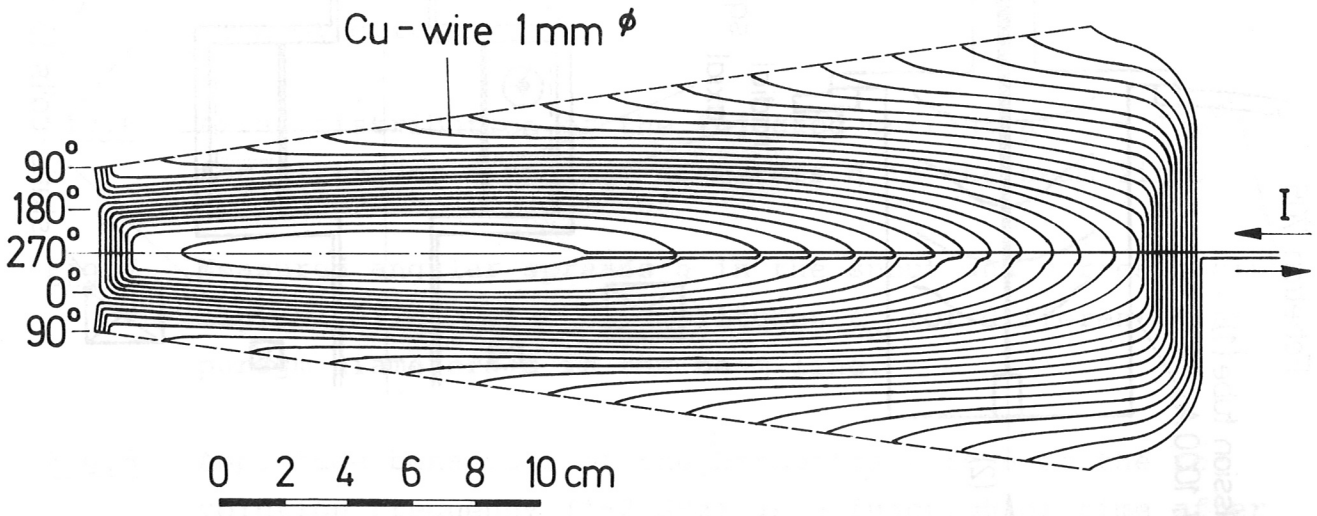
Cu - wire 1 mm ϕ
90°
180°
270°
0°
90°
I
0 2 4 6 8 10 cm

Fig. 3

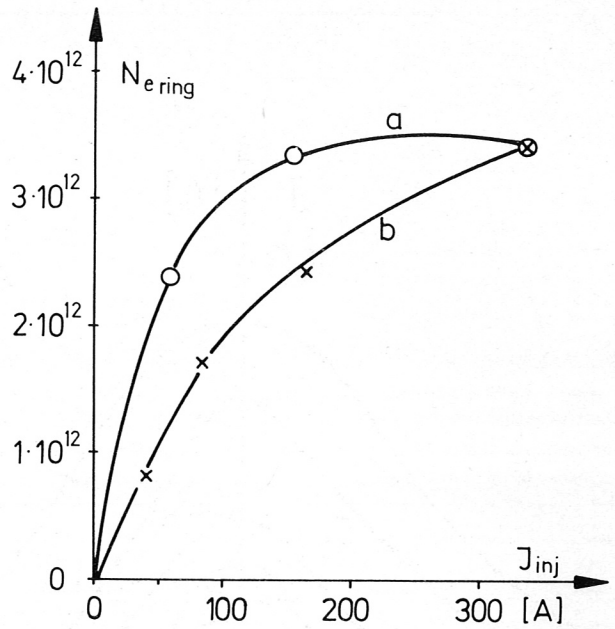
4·10^12
N e ring
3·10^12
2·10^12
1·10^12
0
a
b
J inj
0
100
200
300 [A]

Fig. 4

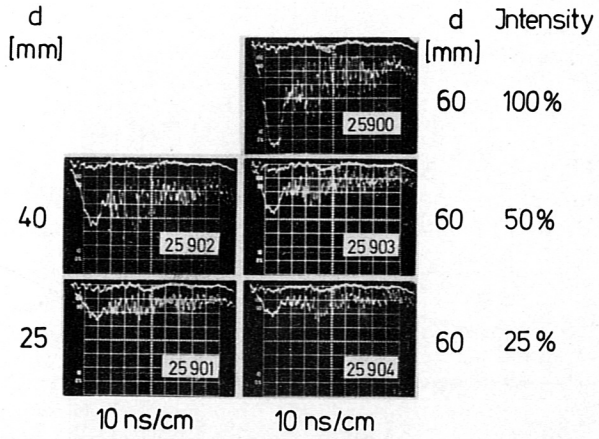
d
[mm]
d
[mm]
Intensity
60
100%
25900
40
25902
25903
60
50%
25
25901
25904
60
25%
10 ns/cm
10 ns/cm

Fig. 5

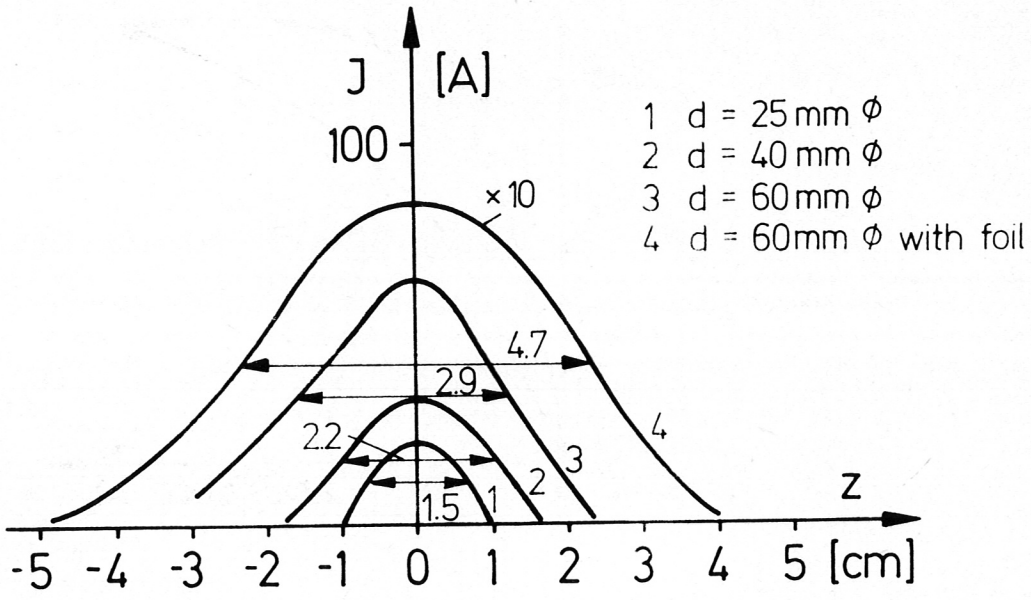
J [A]
100
× 10
1 d = 25 mm ϕ
2 d = 40 mm ϕ
3 d = 60 mm ϕ
4 d = 60 mm ϕ with foil
4.7
2.9
2.2
1.5
1
2
3
4
z
-5 -4 -3 -2 -1 0 1 2 3 4 5 [cm]

Fig. 6

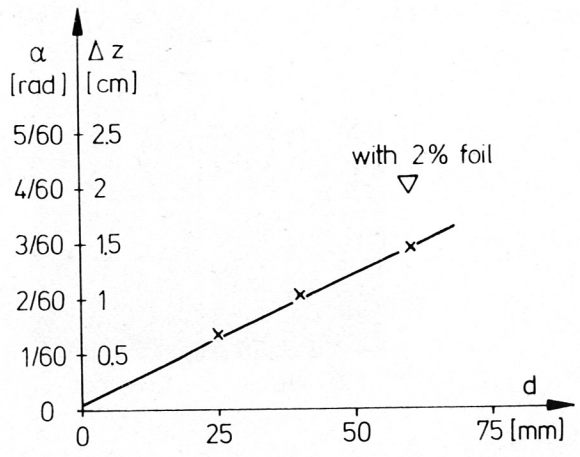
α [rad]
Δ z [cm]
5/60 2.5
4/60 2
3/60 1.5
2/60 1
1/60 0.5
0
with 2% foil
d
0 25 50 75 [mm]

Fig. 7

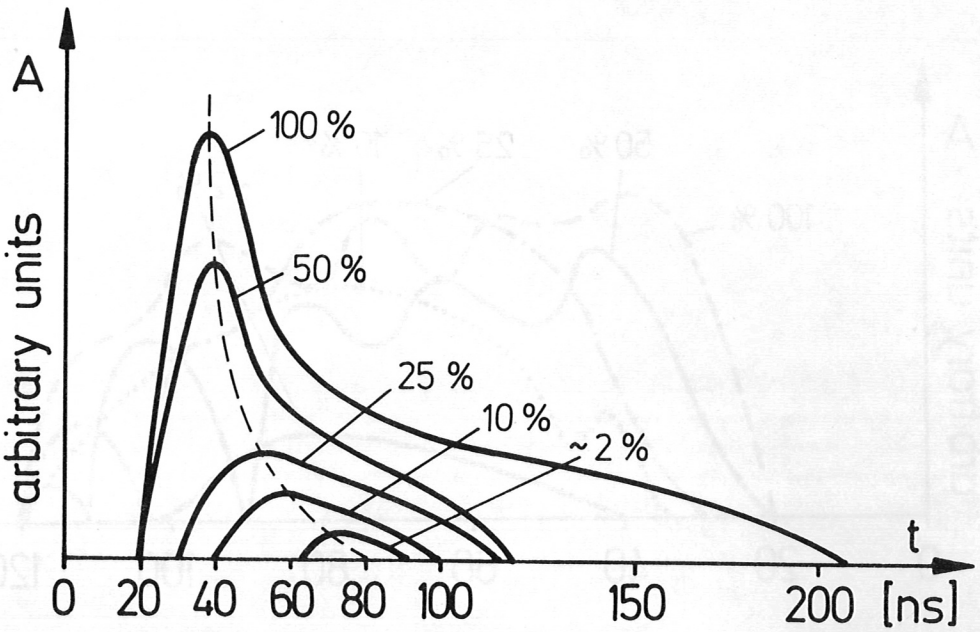
A
arbitrary units
100 %
50 %
25 %
10 %
≃2 %
t
0 20 40 60 80 100 150 200 [ns]

Fig. 8a

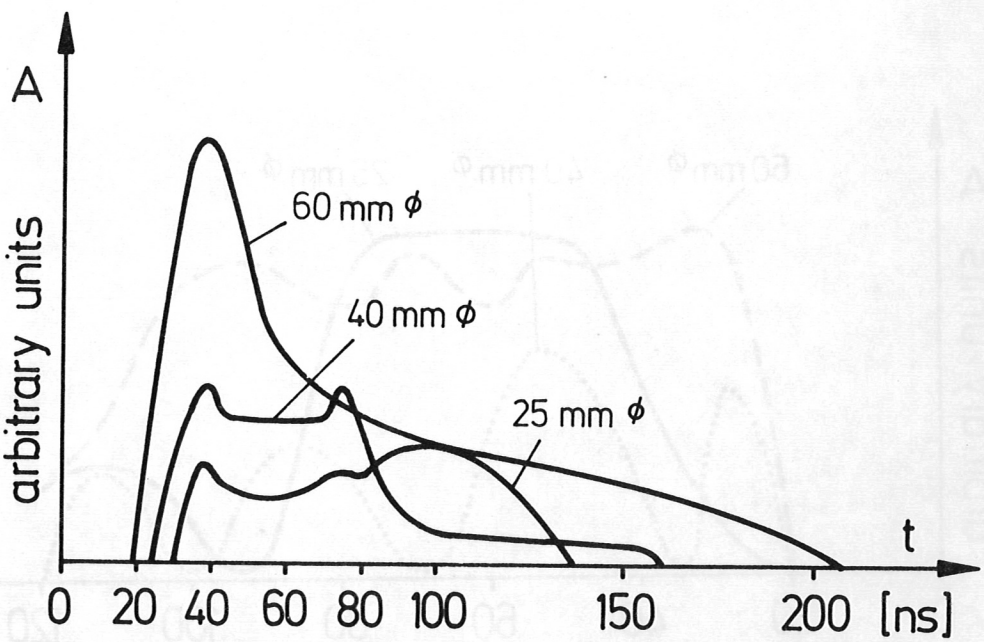
A
arbitrary units
60 mm ϕ
40 mm ϕ
25 mm ϕ
t
0 20 40 60 80 100 150 200 [ns]

Fig. 8b

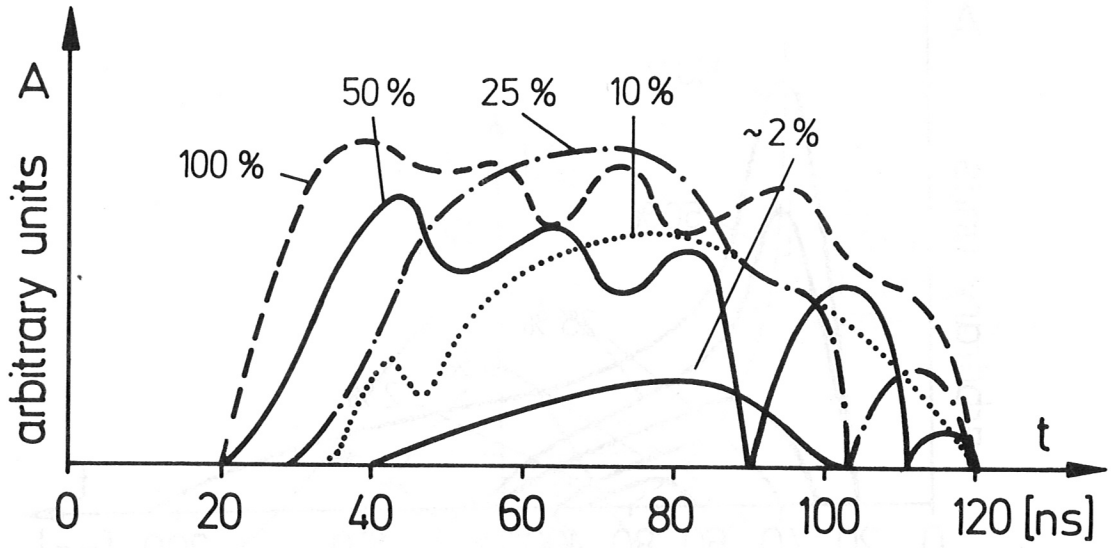
A
arbitrary units
100 %
50 %
25 %
10 %
~2 %
t
0
20
40
60
80
100
120 [ns]

Fig. 9a

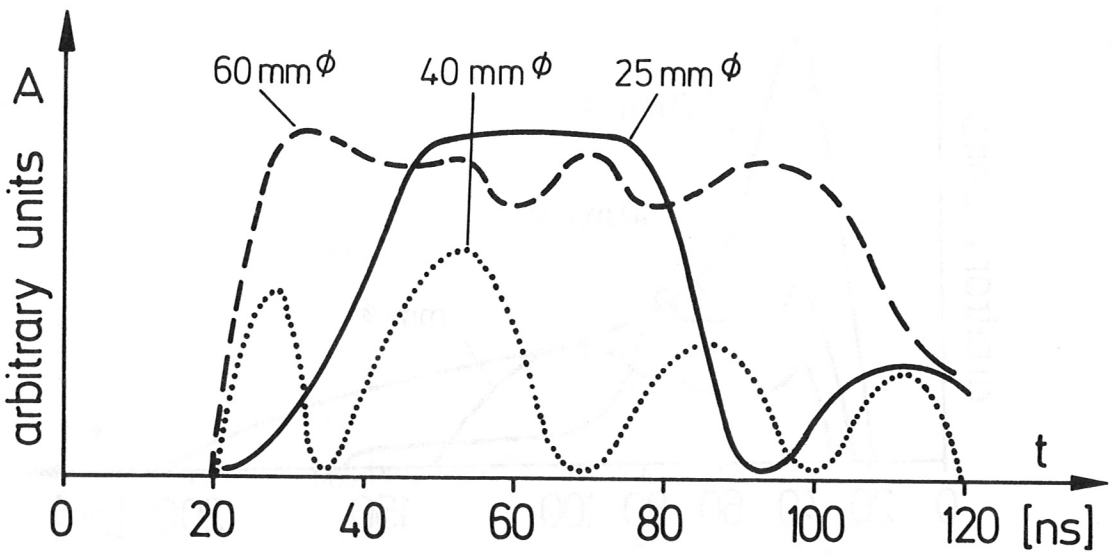
A
arbitrary units
60 mm ϕ
40 mm ϕ
25 mm ϕ
t
0
20
40
60
80
100
120 [ns]

Fig. 9b